EVOLUTION OF MICROSTRUCTURE AND DYNAMIC RECOVERY LEVEL OF Al-Mg-Si-Mn ALLOYS DURING HOT COMPRESSIVE DEFORMATION

Xiaoguo WANG[1,3], Zebing XING[1], Jian QIN[2,3*], Fangzhen LIU[2,3], Hiromi NAGAUMI[2,3*]

As excellent recrystallization resistance of α-Al(MnFe)Si dispersoids and favorable in strength, Mn was added to wrought Al-Mg-Si alloys in recent years. In this study, hot compression tests of 6061 alloy and a Mn containing Al-Mg-Si alloy (HSW-1) were carried out at temperature range from 300 to 500 °C with strain rang from 0.5 to 1.2 at a strain rate of 0. 1 s^{-1} to investigate their hot deformation behaviors. EBSD inverse pole figures were employed to study evolution of microstructure and influence of α dispersoids on dynamic softening mechanism of both alloys. Dynamic recovery (DRV) is predominant softening mechanism of both alloys, and its level is further understood via the help of grain orientation spreads maps (GOS). GOS maps of both deformed alloys were characterized with multi-peaks indicating DRV occurs multiple times during hot processing. This phenome is becoming obvious with decreasing of deformation temperature and increasing of strain. With presence of α dispersoids, the migration of subgrain boundaries was strongly restrained and also substructures rotation. Therefore, there were less peaks in GOS maps of HSW-1 alloy as the reason of α dispersoids which restrains DRV level and retards dynamic recrystallization.

Keywords: α-Al(MnFe)Si dispersoid; dynamic softening; grain orientation spread; substructure rotation; Al-Mg-Si alloys

1. Introduction

6xxx Al alloys have been extensively applied in various industrial applications, including transportation and aerospace, as their excellent formability as well as remarkable weight reduction. With rapid development of new energy vehicles, high strength, high toughness and high fatigue resistance of 6xxx alloys are urgently needed. Substructures have been reported to retard propagation of fatigue cracks and promote dynamic precipitation, which enhances various alloys'

[1] College of Engineering, Shanxi Agricultural University, Taigu, Shanxi, China, e-mail: wxg315550@163.com
[2] Shagang School of Iron and Steel, Soochow University, Suzhou, Jiangsu, China, e-mail james.qin@suda.edu.cn
[3] High Performance Metal Structural Materials Research Institute, Soochow University, Suzhou, Jiangsu, China

mechanical properties [1,2]. Hence, refining substructure size in Al-Mg-Si-Cu alloys favor to gain excellent combination property simultaneously. Hot deformation is an indispensable step in the process of manufacturing Al components which including rolling, extrusion and forging, which plays a vital role on microstructure evolution and determines final mechanical properties of alloys. Hot deformation microstructure of Al alloys is predominated by operative dynamic softening mechanism which mainly refers to DRV or DRX. Although, DRX was reported during hot deformation of Al alloys [3,4], DRV is the preferentially initiated softening mechanism of aluminum alloys in hot processing due to their high stacking fault energy, which resulting in formation of abundant substructures [5,6]. It was reported, the addition of Mn can promote the precipitation of α-Al(MnFeCr)Si dispersoids which can improve recrystallization resistance and retard subgrain boundaries migration ascribed to the Zener dragging force [7–10]. Deforming by proper hot processing parameters of Al-Mg-Si-Cu alloy with HSW-1 is considered a potential technique for producing ultra-fine substructure. So it's necessary to study the effect of α dispersoids on evolution of microstructure and DRV level.

Flow curve mainly consists of two stages, one is controlled by work hardening in which stress increases rapidly, at another stage flow curve reaches a dynamic balance between work hardening and softening mechanism. Flow curves are also often utilized to construct processing maps and constitutive equations to study hot deformation behaviors of Al alloys [11–13]. Most studies mainly focus on the constitutive analysis, relation between deformation parameters and evolution of microstructure and predominant dynamic softening mechanism in processing maps [11,14,15]. Flow stress curves of hot deformed metals predominated by the DRV and DRX were different. Owing to strong softening effect, the occurrence of DRX will lead to a drop in the flow stress demonstrating in the form of a single peak or multiple peaks in flow stress curves. Flow stress curve with multiple peaks will transform into single peak curve associate with increasing of strain rate or decreasing of deformation temperature [16]. Each peak in the flow stress with multiple peaks represents a recrystallization period. Hence, DRX is consisted of a series of recrystallization periods [17]. Flow stress dominated by DRV always exhibited rather flat compared to that of DRX mechanism. So DRV level can be only revealed by microstructure characterization. Nuclei of recrystallized grains can only grow from the subgrains with high misorientation angle to adjacent material due to necessary mobility of substructure [18,19]. Humphreys and Hatherly [20] reported that mobility of grain boundaries with high angle (>15°) was about 100-1000 times than that of substructure with low angle (2-5°). But there is rare information and detailed exploration for evolution of DRV level during hot processing.

In the present study, α dispersoids containing HSW-1 alloy and 6061 alloy

were systematically compared to understand DRV evolution during hot deformation via isothermal compression deformation under various conditions. Electron backscattering diffraction (EBSD) mapping and grain orientation spreads maps (GOS) were applied to characterize grain orientation spread evolution of both alloys during dynamic softening process. A novel approach to understanding of DRV level was proposed and the effect of deformation parameters and α dispersoids on microstructural evolution and DRV level was studied.

2. Experimental

Ingots of 6061 and HSW-1 Al alloys with diameters of 150 mm were used in the present study which were manufactured by direct chill casting. The 6061 and HSW-1 alloys were homogenized at 555 °C for 6 h and 530 °C for 6 h with a heating rate of 2 °C/s, respectively. As initial material, their chemical compositions were listed in Table 1 which conducted by Spectrolab optical emission spectroscopy. The distribution of α dispersoids in the alloys was revealed by etching in 0.5 wt.% HF solution for 20 s at room temperature. The compression tests were performed via a Gleeble 3500 thermo-mechanical simulation unit deformed at a range of 300 to 500°C with strain rate of $0.1s^{-1}$. The cylindrical samples with 10 mm in diameter and 15 mm in height were utilized in present study which were taken from the position with 0.5 times of ingot's radius distance to center of ingot. The samples were heated to temperature with heat rate of 5 °C/s, and then held for 2 minutes to eliminate temperature gradient. Thermal couple was welded on the surface in the middle of the sample. Graphic foils were placed on each side of the sample for lubrication. Then the samples were immediately quenched into water at ambient temperature after compression to preserve the deformed microstructures. Central part of the cross-sections parallel to the compression direction of the specimens were taken for microstructural characterization. Strain-free surfaces for EBSD analysis were prepared by electropolished in 10 wt.% perchloric acid/90 wt.% ethanol. In EBSD measurements, high angle boundaries (HABs) are defined as misorientations larger than 15° and shown as black lines, while low angle boundaries (LABs) are defined as misorientations between 2° and 15° and expressed as white lines. The microstructure of deformed samples was characterized via a transmission electron microscope (TEM, JEOL JEM-2100F). The TEM thin foils were prepared by the twin-jet electropolishing method etched at -20 °C and 20V in a solution of 75 vol.% methanol and 25 vol.% HNO_3.

Table 1

Chemical compositions of HSW-1 and 6061 Al alloys (wt.%)

Alloy	Mg	Si	Cu	Mn	Cr	Fe	Ti	Al
HSW-1	0.9	1.0	0.45	0.48	0.3	0.12	0.02	Bal.
6061	0.68	1.06	0.25	0.02	0.17	0.16	0.03	Bal.

3. Results and discussion

During homogenization heat treatment, different volume fraction of nanoscale α-Al(Mn,Cr)Si dispersoids precipitated in 6061 and HSW-1 alloys. But it's difficult to observe α dispersoids by an optical microscopy as their fine size. After etching by HF solution, the areas with high density of dispersoids would display a bright color in the dark field images. Hence, to reveal the distribution of α dispersoids by OM in present study, the samples were polished and etched and their dark-field images are shown in Fig. 1. There are a few of undissolved coarse microscale primary Mg2Si particles distribute at grain boundaries of both alloys. Nanoscale α-Al(Mn,Cr)Si dispersoids were found in the interior of the grains of both alloys but with significantly different distribution trend. It's obvious, α dispersoids distribute uniformly in HSW-1 alloy which have higher volume fraction and finer diameter as shown in Fig.1(b). Meanwhile in 6061 alloy, there are uneven distribution limited α dispersoids distribute between dendrite arms due to lacking in essential element of Mn.

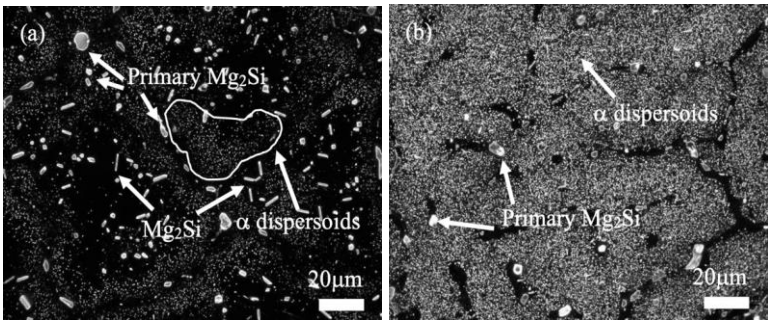

Fig. 1. Optical darkfield microscopy images of (a) 6061 and (b) HSW-1 alloys etched by HF solution.

To further characterize the α dispersoids which precipitate during homogenization heat treatment, transmission electron microscope (TEM) was applied, and TEM images of both alloys were shown in Fig. 2. TEM pictures measurements show the presence of α dispersoids with average equivalent diameter of 364±75 nm and 129±33 nm in 6061 and HSW-1 alloys, respectively. So the α dispersoids precipitate in HSW-1 alloy have not only higher volume fraction and uniform distribution but also have much finer size.

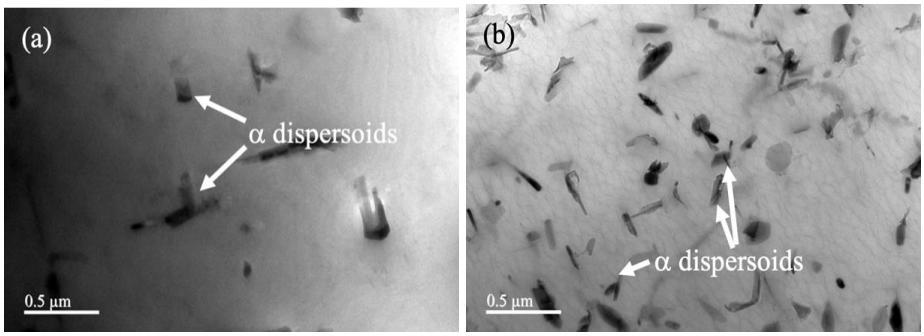

Fig. 2 TEM images of α dispersoids in homogenized 6061 alloy (a) and HSW-1 alloy (b).

The flow stress curves of both alloys deformed under different conditions are shown in Fig. 3. At initial stage of deformation, stress increases rapidly resulting from work hardening for all curve, and then it gradually reaches to the peak value causing by activation of dynamic softening process, i.e., DRV or DRX. After that, flow stress curves exhibit a steady state indicating dynamic equilibrium between work hardening and dynamic softening process is achieved. There is no obvious decreasing of flow stress after reaching maximum value, indicating DRX is not the principal mechanism for both alloys. But it's difficult to analysis DRV level or substructures evolution simply by constitutive equations and processing maps only base on flow stress behaviors. It should be noticed that the HSW-1 alloy has a higher flow stress than 6061 alloy at all deformation conditions due to the presence of α dispersoids.

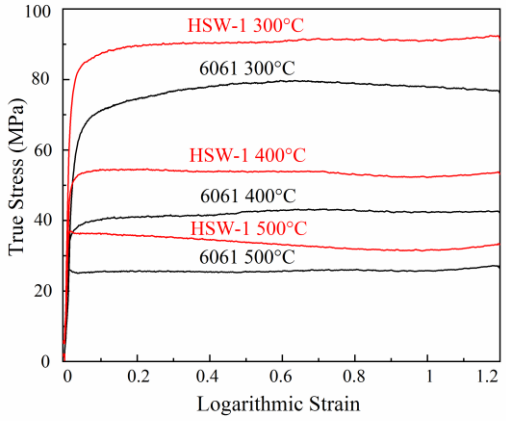

Fig. 3 True stress-strain curves of 6061 and HSW-1 alloys deformed at temperature range from 300 °C to 500 °C with a strain rate of 0.1s-1.

As shown in Fig. 4 are inverse pole figures (IPFs) of EBSD measurements for both alloys after deformation at 400 °C with strain rate of 0.1 s-1 to a strain

range from 0.5 to 1.2. The IPF map and compression direction (CD) are shown in Fig. 4 (g). So, the color difference of adjacent sub-grains represents misorientation between them [21]. It is obvious that substructures fully develop and homogenously distribute throughout deformed grains of both alloys, indicating DRV is predominate mechanism. During hot deformation, substructure size barely changes and low angle boundaries transfers to medium or high angle boundaries via substructure rotation. This phenomenon was reflected on IPFs as obvious color difference between substructures and their adjacent ones which were marked by black arrows. Associate with increasing of strain, misorientation between substructures was aggravated and high angle boundaries (>15°) or recrystallized grains formed which were marked by black frames. Meanwhile in HSW-1 alloy, although substructure size is almost same as 6061 alloy, misorientation of substructures is much less than that of 6061 alloy. It indicates that rotation of substructure is limited by α dispersoids which act as obstacles and restrain mobility of sub-grain boundaries effectively.

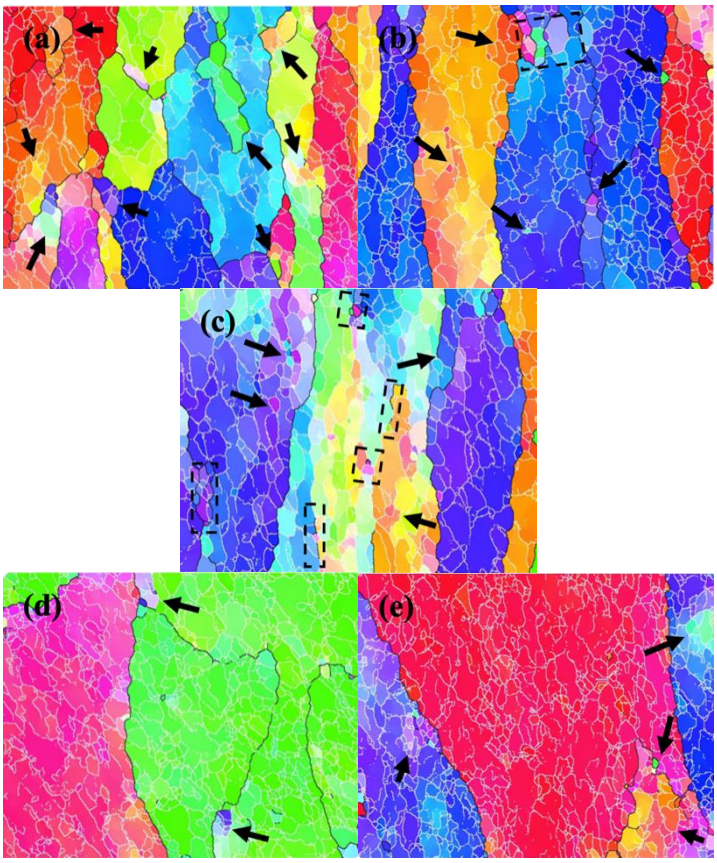

Fig. 4.1. Sub-structures of 6061 alloy (a), (b) & (c) and HSW-1 alloy (d), (e) & (f) deformed at 400 °C with strain rate of 0.1 s-1 to stain of (a) & (d) 0.5, (b) & (e) 0.8 and (c) & (f) 1.2 and inversed pole figure with compression direction (CD) (g)

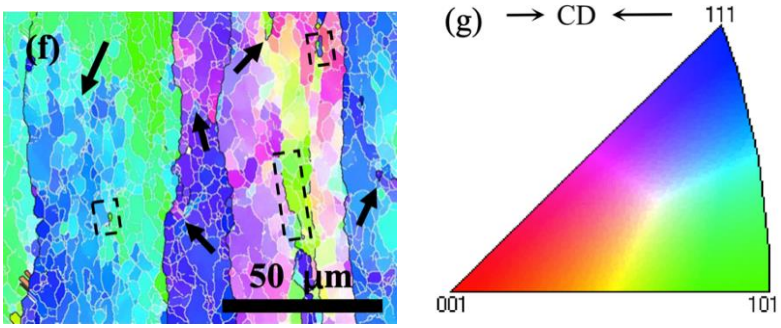

Fig. 4.2. Sub-structures of 6061 alloy (a), (b) & (c) and HSW-1 alloy (d), (e) & (f) deformed at 400 °C with strain rate of 0.1 s-1 to stain of (a) & (d) 0.5, (b) & (e) 0.8 and (c) & (f) 1.2 and inversed pole figure with compression direction (CD) (g).

Fig. 5 presents the evolution of substructure as a function of deformation temperature of both alloys. It is apparent that substructure size increases with increasing of deformation temperature for both alloys. It indicates subgrain boundaries migration is a thermally activated process. Microstructure of both alloys deformed at 300 °C was characterized by massive substructure with similar orientation within deformed initial grains. Besides that, substructure rotation is also observed in both alloys, where are pointed by black arrows in Fig. 5 (a)& (d). The color differences within deformed initial grains of both alloys are intensified when the deformation temperature increases to 400 °C (Fig. 5 (b)& (e)), which means substructure rotation is also promoted. A further increment of 100 °C in deformation temperature results in obvious transformation of LABs to HABs and formation of recrystallized grains where are marked in black boxes (Fig. 5 (c) &(f)). Recrystallized grains in 6061 alloy dramatically coarse and transfer from elongated ones (Fig. 5 (b)) to equiaxed ones (Fig. 5 (c)) associate with increasing of deformation temperature. Compared to 6061 alloy, substructure rotation in HSW-1 alloy was restrained as shown in Fig. 5 (e).

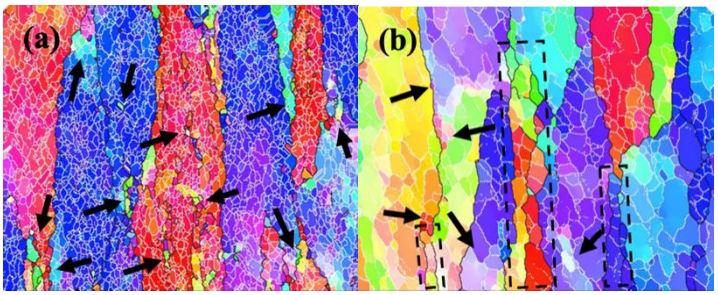

Fig. 5.1. Sub-structures of 6061 (a, b & c) and HSW-1 (d, e & f) alloys deformed at 300 °C, 400 °C and 500 °C, respectively, with 0.1 s-1 to stain of 1.2.

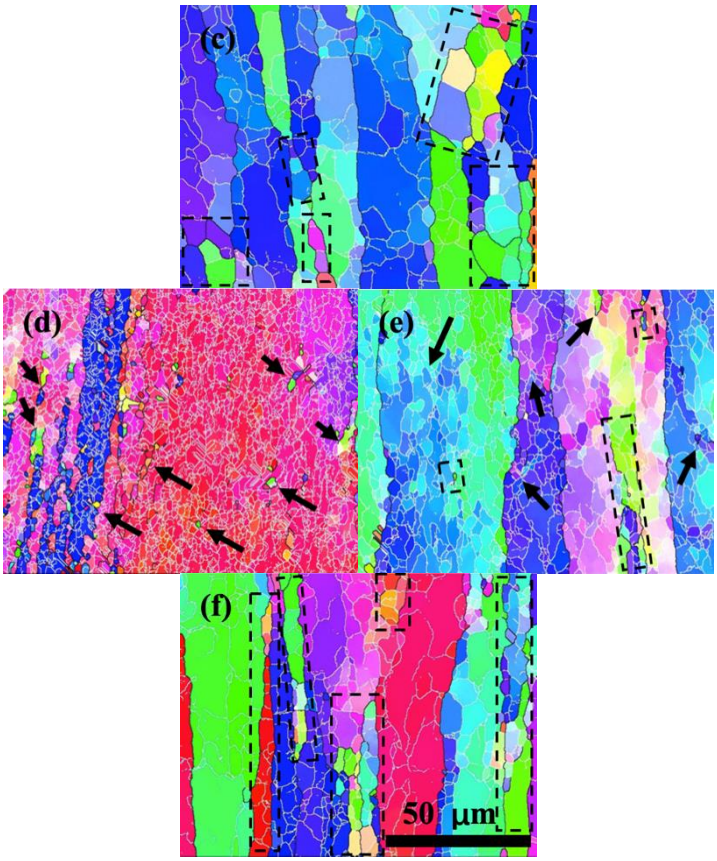

Fig. 5.2. Sub-structures of 6061 (a, b & c) and HSW-1 (d, e & f) alloys deformed at 300 °C, 400 °C and 500 °C, respectively, with 0.1 s-1 to stain of 1.2.

Besides that, recrystallized grains in HSW-1 alloy are less and finer than that of 6061 alloy and still maintain elongated shape. All of these proving that α dispersoids can not only restrain migration of substructures but also inhibited growth of recrystallized grains.

Evolution of subgrain boundaries in HSW-1 alloy as a function of deformation temperature is shown in Fig. 6. It can be found that α dispersoids effectively pin dislocations and subgrain boundaries. The subgrain boundaries of alloy deformed at 300 °C is tangled dislocations (Fig. 6 (a)). With deformation temperature increasing to 400 °C subgrain boundaries transfers to dislocation clusters (Fig. 6 (b)). When the alloy deformed at 500 °C, interference stripes of equal thickness is found at subgrain boundaries (Fig. 6 (c)), indicating there is high angle misorientation between adjacent subgrains. It can be concluded that misorientation of subgrain boundaries increases with increasing of deformation temperature.

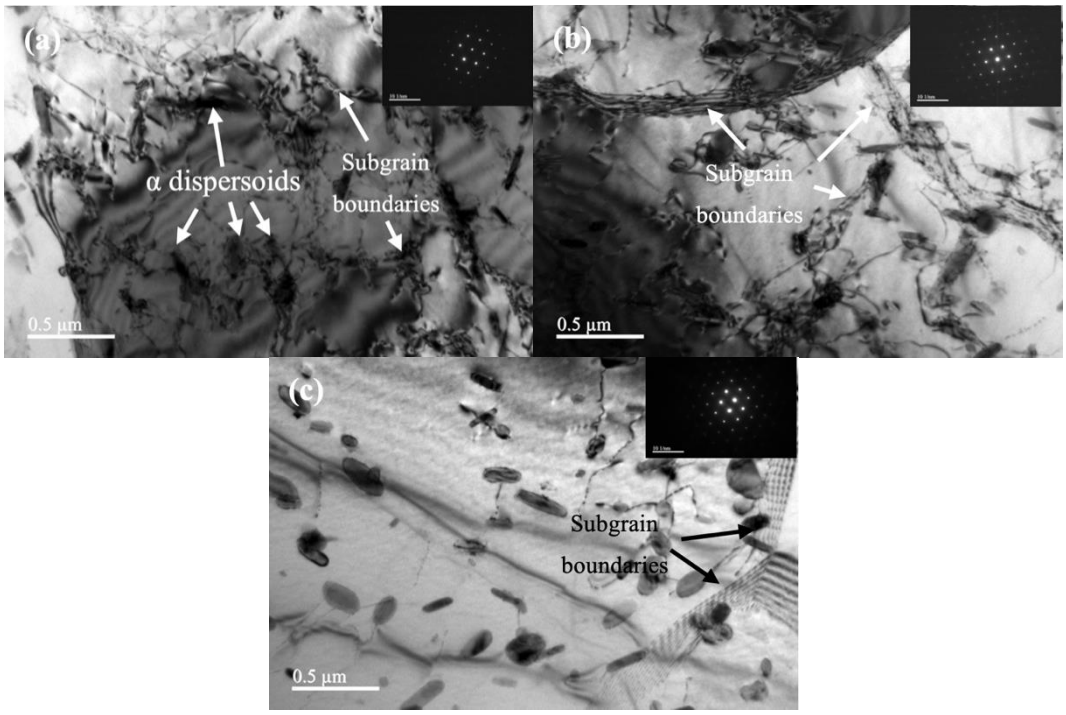

Fig. 6 Microstructure of HSW-1 alloy deformed at temperatures of 300 °C (a), 400 °C (b) and 500 °C (c).

DRX processing level of the alloy are normally expressed by recrystallization fraction which were characterized by EBSD measurements. But DRV level can't be easily presented only by evolution of substructures misorientation or their size. To understand the effect of deformation conditions on DRV level, grain orientation spread maps (GOS) of LABs was utilized. The GOS of both alloys at various deformation strain was shown in Fig. 7 in which multiple peaks are noticed and marked by dash lines. Generally, there are 3 peaks distribute at around 1.8°, 3.6° and 5.5° in all GOS at three strains. At initial stage of deformation process, the generation and multiplication of dislocations promoted the dislocation reaction then formed abundant substructures, which with similar misorientation concentrated at a low angle. With increasing of strain, number fraction of these substructures increases and reaches to a peak value at which accumulated stored energy is high enough to active transformation of substructure boundaries to higher angle boundaries. Then, substructures begin to rotate by dislocation annihilation and relaxation, which is similar to progress of static recovery. It will lead to decreasing of number fraction of substructures and increasing of misorientation angle. As there is a dynamic balance between work hardening and DRV/DRX, these processes mentioned above will repeat several times with further increasing of strain. These peaks are evidence and trace of occurrences of

multiple times substructures rotations which promotes substructures' misorientation transfers higher angles. Substructures with high angles are more easily transfer to high angle boundaries or recrystallized grains since their mobility is significantly greater than that of substructures with lower angles [20]. Hence, the number fraction of the peaks at higher misorientation are lower than that at lower misorientation as shown in Fig. 7. Besides that, number fraction of first peak at 1.8° decreases associate with increasing of strain. It's because of more substructures transfer to higher misorientation, which cause increasing of number fraction at 3.6° and 5.5° and decreasing at 1.8° with increasing of strain, as shown in Fig. 7 (a). Meanwhile, due to pinning effect of α dispersoids, migration of dislocation and substructures were strongly inhibited. So, the rotation of substructures barely occurred and no obvious misorientation peaks were found in Fig. 7 (b). The substructures rotation and transformation from low angles to high angles can be found in Fig. 4 according to the description above.

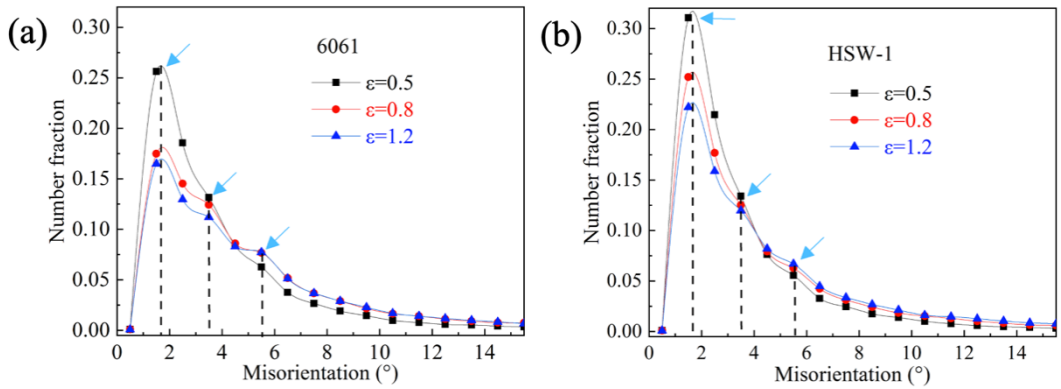

Fig. 7 Grain orientation spread of LABs for 6061 (a) and HSW-1 (b) deformed at 400 °C with strain rate of 0.1 s-1 to different strains.

As presented in Fig. 8 is the evolution of GOS of 6061 and HSW-1 alloys as a function of deformation temperatures which shows a similar tendency as Fig. 7. There are also three peaks site at similar angle in all GOS of three deformation temperatures. Compared to strain, deformation temperature has significantly influence on substructures evolution. With decreasing of deformation temperature, the tendency of peaks in GOS becomes obvious, especially at 300 °C (Fig. 8 (a)). The misorientation peak at 3.6° and 5.5° are becoming non-obvious with increasing of deformation temperature. It's because of the increasing of deformation temperature provides sufficient thermal energy to promote substructures migration and rotation. So, the substructure size coarsens (Fig. 5 (a)), misorientation of substructures easily transfer to higher angles (Fig. 5 (b)), and even recrystallized (Fig. 5 (c)) which reduce the number fraction these peaks. According to Fig. 5 (d, e & f), the main operative dynamic softening mechanism

for HSW-1 alloy is still DRV. Even deformation temperature was raised to 500 °C, α dispersoids shows promising recrystallization resistance. As shown in Fig. 8 (b), substructure of HSW-1 alloy mainly distributed at peak sited at 1.8°. And so, the effect of temperature on GOS of HSW-1 alloy is not so notable as that of 6061 alloy.

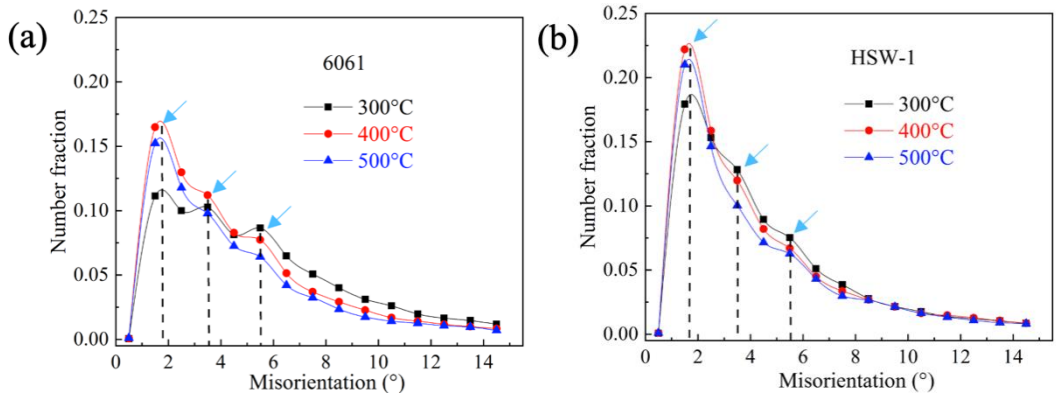

Fig. 8 Grain orientation spread of LABs for 6061 (a) and HSW-1 (b) alloy deformed with strain rate of 0.1 s-1 to a strain of 1.2 at different deformation temperature.

In summary, DRV are the dominant mechanism for both alloys and its level can be generally expressed by the comprehensive description of EBSD measurements and GOS. DRV level of both alloys increases via substructure growth and rotations. The substructure rotation is activated by stored energy and there is a critical value above which the rotation of substructure occurs. The substructures with higher misorientation their boundaries have a greater mobility. It means rotation of substructure is promoted and then reduce the number fraction. Hence, there are peaks in GOS at some misorientations. As the presence of α dispersoids migration of substructures is inhibited and even further restrain their rotation, so the existence of peaks in GOS of HSW-1 alloy is not so obvious as 6061 alloy.

4. Conclusions

Uniaxial compression tests were performed for homogenized 6061 and HSW-1 alloys at temperature range from 300 °C to 500 °C to a strain range from 0.5 to 1.2 with strain rate of 0.1 s-1. Following conclusions were drawn based on microstructure characterization and evolution of GOS at various deformation conditions:

(1) DRV is predominant mechanism for the two studied Al alloys, and it evolves by progressive growth and rotation of substructures.

(2) Grain orientation spread maps are employed to understand

evolution of DRV level during hot processing of Al-Mg-Si alloys. There are several misorientation peaks in GOS, which present multiple times of substructures rotations. The phenomenon of misorientation peaks becomes obviously associate with descending of deformation temperature and increasing of strain.

(3) Presence of α dispersoids effectively restrain migration of dislocation and substructure, hence, inhibit sub-grain rotation. So, misorientation peaks are barely found in GOS of HSW-1 alloy.

Acknowledgements

The authors acknowledge the financial support provided National Natural Science Foundation of China (Grant No. U1864209).

R E F E R E N C E S

[1]. *M. Nakai, G. Itoh,* The effect of microstructure on mechanical properties of forged 6061 aluminum alloy, Mater. Trans. 55 (2014) 114–119.
[2]. *J. Zuo, L. Hou, J. Shi, H. Cui, L. Zhuang, J. Zhang,* Effect of deformation induced precipitation on grain refinement and improvement of mechanical properties AA 7055 aluminum alloy, Mater. Charact. 130 (2017) 123–134.
[3]. *A. Güzel, A. Jäger, F. Parvizian, H.G. Lambers, A.E. Tekkaya, B. Svendsen, H.J. Maier,* A new method for determining dynamic grain structure evolution during hot aluminum extrusion, J. Mater. Process. Technol. 212 (2012) 323– 330.
[4]. *C. Poletti, T. Wójcik, C. Sommitsch,* Hot deformation of AA6082 containing fine intermetallic particles, Metall. Mater. Trans. A Phys. Metall. Mater. Sci. 44 (2013) 1577–1586.
[5]. *J. Hu, J. Teng, X. Ji, D. Fu, W. Zhang, H. Zhang,* Enhanced mechanical properties of an Al-Mg-Si alloy by repetitive continuous extrusion forming process and subsequent aging treatment, Mater. Sci. Eng. A. 695 (2017) 35–44.
[6]. *J. Sarkar, Y.V.R.K. Prasad, M.K. Surappa,* Optimization of hot workability of an Al-Mg-Si alloy using processing maps, J. Mater. Sci. 30 (1995) 2843–2848.
[7]. *R. Guemini, A. Boubertakh, G.W. Lorimer,* Study of the recrystallization process of AlMgSi alloys containing transition elements, J. Alloys Compd. 486 (2009) 451–457.
[8]. *L.P. Troeger, E.A. Starke,* Particle-stimulated nucleation of recrystallization for grain-size control and superplasticity in an Al-Mg-Si-Cu alloy, Mater. Sci. Eng. A. 293 (2000) 19–29..
[9]. *Z. Li, J. Qin, B. Zhang, H. Nagaumi,* Effect of cr addition on microstructure and mechanical properties at elevated temperature of almnmgsi alloys, Mater. Trans. 61 (2020) 2095–2100.
[10]. *X. Wang, J. Qin, H. Nagaumi, R. Wu, Q. Li,* The Effect of α -Al(MnCr)Si Dispersoids on Activation Energy and Workability of Al-Mg-Si-Cu Alloys during Hot Deformation, Adv. Mater. Sci. Eng. 2020 (2020).
[11]. *X. Kai, C. Chen, X. Sun, C. Wang, Y. Zhao,* Hot deformation behavior and optimization of processing parameters of a typical high-strength Al-Mg-Si alloy, Mater. Des. 90 (2016) 1151–1158.
[12]. *Y. Liu, C. Geng, Q. Lin, Y. Xiao, J. Xu, W. Kang,* Study on hot deformation behavior and intrinsic workability of 6063 aluminum alloys using 3D processing map, J. Alloys Compd. 713 (2017) 212–221.
[13]. *R. Hu, T. Ogura, H. Tezuka, T. Sato, Q. Liu,* Dispersoid formation and recrystallization

behavior in an Al-Mg-Si-Mn alloy, J. Mater. Sci. Technol. 26 (2010) 237–243.
[14]. *G. Lin, Z. Zhang, H. Wang, K. Zhou, Y. Wei,* Enhanced strength and electrical conductivity of Al-Mg-Si alloy by thermo-mechanical treatment, Mater. Sci. Eng. A. 650 (2016) 210–217.
[15]. *J. Qin, Z. Zhang, X.-G. Chen,* Hot Deformation and Processing Maps of Al-15%B_4C Composites Containing Sc and Zr, J. Mater. Eng. Perform. 26 (2017).
[16]. *T. Sakai, J.J. Jonas,* Overview no. 35 Dynamic recrystallization: Mechanical and microstructural considerations, Acta Metall. 32 (1984) 189–209.
[17]. *M.J. Luton, C.M. Sellars,* Dynamic recrystallization in nickel and nickel-iron alloys during high temperature deformation, Acta Metall. 17 (1969) 1033–1043.
[18]. *A.H. Cottrell,* Theory of dislocations, Prog. Met. Phys. 1 (1949).
[19]. *R.D. Doherty, D.A. Hughes, F.J. Humphreys, J.J. Jonas, D. Juul Jensen, M.E. Kassner, W.E. King, T.R. McNelley, H.J. McQueen, A.D. Rollett,* Current issues in recrystallization: A review, Mater. Sci. Eng. A. 238 (1997) 219–274.
[20]. *F.J. Humphreys, M. Hatherly,* The Mobility and Migration of Boundaries, Recryst. Relat. Annealing Phenom. (2004) 121–167.
[21]. *Q. Yang, Z. Deng, Z. Zhang, Q. Liu, Z. Jia, G. Huang,* Effects of strain rate on flow stress behavior and dynamic recrystallization mechanism of Al-Zn-Mg-Cu aluminum alloy during hot deformation, Mater. Sci. Eng. A. 662 (2016) 204–213.